

From A to B in free energy space

Davide Branduardi,^{a)} Francesco Luigi Gervasio, and Michele Parrinello
*Computational Science, Department of Chemistry and Applied Biosciences, ETH Zürich, USI Campus,
 Via Giuseppe Buffi 13, CH-6900 Lugano, Switzerland*

(Received 6 November 2006; accepted 18 December 2006; published online 7 February 2007)

The authors present a new method for searching low free energy paths in complex molecular systems at finite temperature. They introduce two variables that are able to describe the position of a point in configurational space relative to a preassigned path. With the help of these two variables the authors combine features of approaches such as metadynamics or umbrella sampling with those of path based methods. This allows global searches in the space of paths to be performed and a new variational principle for the determination of low free energy paths to be established. Contrary to metadynamics or umbrella sampling the path can be described by an arbitrary large number of variables, still the energy profile along the path can be calculated. The authors exemplify the method numerically by studying the conformational changes of alanine dipeptide. © 2007 American Institute of Physics. [DOI: [10.1063/1.2432340](https://doi.org/10.1063/1.2432340)]

I. INTRODUCTION

Sampling rare events and reconstructing the free energy along a path from an initial to a final state is one of the principal goals of computational chemistry, biochemistry, and biophysics. To this end a large number of algorithms have been proposed. Two important classes can be identified. One aims to reconstruct the paths that connect an initial and a final configuration. The other is based on an explicit choice of relevant descriptors for the process of interest. Examples of the first class are the nudged elastic band (NEB),^{1–3} the string method (SM),⁴ transition path sampling (TPS),^{5,6} Vergilius,^{7,8} milestoning,⁹ etc. In the second class we find, to name just a few, thermodynamic integration,^{10,11} umbrella sampling,¹² weighted histogram techniques,^{13–15} steered dynamics,¹⁶ adaptive force bias,¹⁷ conformational flooding,¹⁸ hyperdynamics,¹⁹ taboo search,²⁰ local elevation,²¹ metadynamics,²² and other combined approaches.^{23–25}

Methods that use a small set of collective variables (CVs) for describing the reaction process have been extremely successful²⁶ because of their ability to sample large regions of configurational space, leading to the prediction of unexpected intermediates and metastable states.²⁷ A further advantage of these approaches is that no assumption is made on the final state. However, in many cases finding CVs that take into account all the relevant degrees of freedom is not easy. For instance in problems of great biological interest such as the study of large conformational changes, protein folding, or protein-protein interaction the number of CVs needed in discriminating between different states is too big. This would lead to a very large computational effort, and even if it were possible to evaluate the corresponding multi-dimensional free energy surface (FES) its interpretation would be too difficult. Thus when the initial and the final states are known the use of path based schemes is very

tempting. Their usefulness has been amply proved^{1,4,6} in the search for reaction paths and transition states on the potential energy surface (PES).^{28–30}

At finite temperature, which is the case of interest here, methods based on the study of PES (Refs. 1 and 4) are not applicable since entropic effects become relevant. In this regime among the path methods only TPS (Ref. 5) and the finite temperature string method^{31,32} appear to be viable approaches. In the first case dynamical trajectories are generated but free energy informations require separate calculations. Furthermore sampling becomes inefficient if the reaction time is large unless further assumptions are done³³ and defining a suitable reaction coordinate often becomes difficult. A different approach has been taken in Ref. 31. Here rather than looking at individual trajectories one focuses on the average flux of reactive trajectories that connects reactants and products. Under appropriate circumstances this flux can be described as a tube in configuration space. The tube center gives the reaction coordinate and results from the average over all reactive trajectories. The tube width is to be related to fluctuations around this averaged trajectory. A variational procedure for finding the reaction coordinate is also given.³¹

A difficulty common to all path based methods, be it at zero or finite temperature, is that they are local in the space of reactive paths. It is in fact possible for a given system to go from the initial to the final configurations via qualitatively different paths which are separated by large energy barriers. In fact by local moves it is difficult generate paths which are separated from the initial guess by large energy or free energy barriers. Overcoming these barriers requires implementing non local optimization methods which add an extra and highly non trivial layer of complexity to the problem.

In the spirit of Ref. 31 we introduce a novel method for finding low free energy paths. We work on the free energy surface and combine path approaches with the use of CVs thus allowing exploration of large configurational space extending the search to low energy paths which lie in a very

^{a)}Author to whom correspondence should be addressed. Electronic mail: davide.branduardi@phys.chem.ethz.ch

different basin from the initial one. In this way we will be able to find interesting intermediates. Furthermore if conditions are right, namely if analysis of Ref. 31 can be applied, the low free energy path obtained will define the system reaction coordinate.

In order to do this we define a putative reaction coordinate and two CVs which are functions of it. The latter are simple to implement and divide the space into multidimensional isosurfaces. In the proximity of the initial guess one set of isosurfaces reduces to planes orthogonal to it. The other ensemble of isosurfaces describes the locus of points which are equidistant from the guessed reaction coordinate thus forming a tube that surrounds it. The FES relative to these two collective variables provides information not only on the low free energy path close to the initial guess but also on other qualitative different paths which can be separated from the initial one by large barriers. In addition to this ability of exploring in a very nonlocal way different low energy paths the formalism can be used to establish a variational principle. This gives the key for optimizing locally a path in a computationally expedite manner.

We applied this method to the case of alanine dipeptide in vacuum, and we studied the transition between $C_{7\text{eq}}$ and C_{ax} conformers^{34–36} at room temperature. The method finds that there are three different low energy paths. The calculation is started with a rather primitive guess for the path then with our method all the possible low free energy paths are found and refined such that accurate results are obtained for all of them with a relatively modest computational effort.

II. METHOD

We assume that the transition to be studied can be described by a set of coordinates \mathbf{R} which we arrange to form a multidimensional vector representing the putative reaction coordinate. Contrary to the case of metadynamics the number N of coordinates used can be rather large. For instance they could be a subset of atomic coordinates, say, the C_α of a protein or in other circumstances more complex functions of the atomic coordinates such as those that are aimed at describing solvation properties.^{37,38} Our goal is to estimate the low free energy path that connects an initial state \mathbf{R}_A to a final state \mathbf{R}_B . In this space we guess an initial reaction coordinate which we express parametrically in the form $\mathbf{R}(t)$. The parametrization is such that $\mathbf{R}(0)=\mathbf{R}_A$ and $\mathbf{R}(1)=\mathbf{R}_B$. We now introduce two functions of the reaction coordinate \mathbf{R} ,

$$s(\mathbf{R}) = \lim_{\lambda \rightarrow \infty} \frac{\int_0^1 t e^{-\lambda(\mathbf{R} - \mathbf{R}(t))^2} dt}{\int_0^1 e^{-\lambda(\mathbf{R} - \mathbf{R}(t))^2} dt} \quad (1)$$

and

$$z(\mathbf{R}) = \lim_{\lambda \rightarrow \infty} -\frac{1}{\lambda} \ln \int_0^1 e^{-\lambda(\mathbf{R} - \mathbf{R}(t))^2} dt. \quad (2)$$

These two functions define isosurfaces of dimension $N-1$ that have very useful properties. They derive from the fact that for $\lambda \rightarrow \infty$ the dominant contribution to the integrals comes from the values t_0 for which $(\mathbf{R} - \mathbf{R}(t))^2$ is minimal.

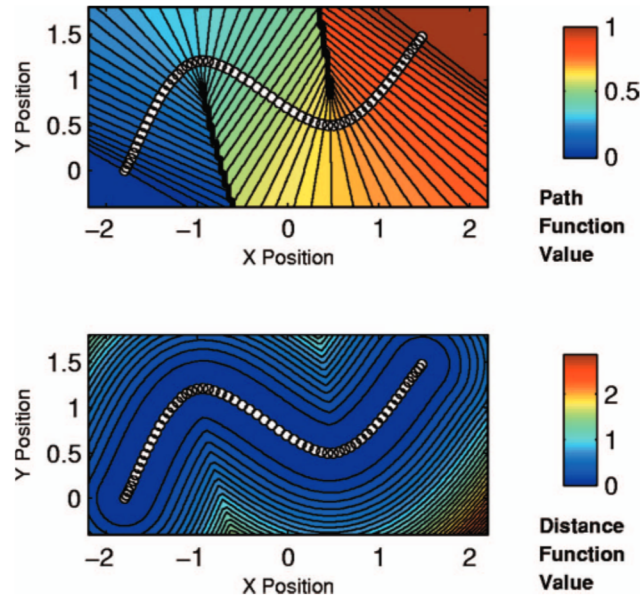


FIG. 1. (Color) Surface plot of Eq. (1) (top) for sixty points in two dimensions. The measure of the distance $(\mathbf{R} - \mathbf{R}(t))^2$ has been replaced with the Cartesian square distance from each white dot. Note that isolines are perpendicular to the path in its neighborhood. Bottom: Contour plot of Eq. (2) in two dimensional space shows that the definition of z can be approximately considered as a measure of the distance from the path itself.

As can be seen in Fig. 1 close to $\mathbf{R}(t)$ the isosurfaces defined by $s(\mathbf{R})=s$ for $0 < s < 1$ are well approximated by planes orthogonal to the curve $\mathbf{R}(t)$.

Instead the isosurfaces $z(\mathbf{R})=z$ define the set of points which are at square distance z from the putative reaction coordinate thus forming a tube that wraps around $\mathbf{R}(t)$. As we move away from the neighborhood of $\mathbf{R}(t)$, that is to say, for large values of z the isosurface $s(\mathbf{R})$ ceases to be planar due to curvature of the path. However, we expect that for most physically relevant trajectories and for large N the isosurfaces remain planar for large values of z . Thus the use of $s(\mathbf{R})$ and $z(\mathbf{R})$ provides a simple and computationally efficient means of constructing two important geometrical surfaces associated to a given curve $\mathbf{R}(t)$. Of course in practical applications the limit $\lambda \rightarrow \infty$ needs not to be taken explicitly and it suffices to take large enough λ . Before proceeding farther we cannot help noting the amusing formal similarity between $z(\mathbf{R})$ and the free energy of a hypothetical statistical mechanical system whose “temperature” is $1/\lambda$ and whose partition function is $Z = \int_0^1 e^{-\lambda(\mathbf{R} - \mathbf{R}(t))^2} dt$. Likewise Eq. (1) can be interpreted as the expectation value of t over the same ensemble.

With these CVs we can proceed to the construction of the free energy surface $F(s, z)$ which is defined modulo an additive constant as

$$F(s, z) = -\frac{1}{\beta} \ln \langle \delta(s - s(\mathbf{R})) \delta(z - z(\mathbf{R})) \rangle, \quad (3)$$

where the average is taken over the Boltzmann distribution. This can be done with any convenient statistical mechanical method such as umbrella sampling¹² or metadynamics.²² An illustrative example of the nature of such surface is given in the A panel in Fig. 4 which has been evaluated for a realistic

model to be described below. It is seen that the surface exhibits a number of valleys that connect the initial and final states. They correspond to different possible low free energy reaction coordinates. The path which is closest to the initial guess $\mathbf{R}(t)$ is the one closest to the $z=0$ line, but other different low energy paths can be identified. It is this feature that gives to the method the ability of finding low free energy paths qualitatively different from the initial guess.

We postpone to later the discussion of this important issue. For the time being we focus on an efficient procedure for improving locally the initial guess $\mathbf{R}(t)$. We note that if $\mathbf{R}(t)$ were the minimum free energy path the $z=0$ line would be a good approximation to its mapping on the (s,z) plane. This is clearly not true in the example of Fig. 4. We can still use the locus of the minima in the valley closest to the $z=0$ line to get a rough estimate for this low free energy path. Here we suggest a variant of the procedure introduced and formally justified in Ref. 31 in which the planes orthogonal to a guessed path $\mathbf{R}(t)$ are constructed and in these planes the closest free energy minima are located. The set of these points gives the lowest free energy path. Here we turn this approach upside down and propose a different method. To this effect we introduce the string tension $\mathcal{T}[\mathbf{R}(t)]$ which is a measure of the deviation of $\mathbf{R}(t)$ from the closest minimum free energy path,

$$\mathcal{T}[\mathbf{R}(t)] = \int_0^1 ds F(s,0). \quad (4)$$

This is a functional which depends on the path $\mathbf{R}(t)$ via its role in the definition of the variables $s(\mathbf{R})$ and $z(\mathbf{R})$ in Eqs. (1) and (2) and has a local minimum whenever $\mathbf{R}(t)$ is a low free energy path. This leads to the variational principle:

$$\frac{\delta \mathcal{T}[\mathbf{R}(t)]}{\delta \mathbf{R}(t)} = 0, \quad (5)$$

which is subject to the boundary conditions $\mathbf{R}(0)=\mathbf{R}_A$ and $\mathbf{R}(1)=\mathbf{R}_B$. As the minimization proceeds the function $s(\mathbf{R})$ and $z(\mathbf{R})$ which depend on $\mathbf{R}(t)$ vary and during minimization $\mathbf{R}(t)$ needs to be reparametrized as is done, for instance, in methods such as NEB (Refs. 1 and 2) or SM.^{4,31}

It has to be noticed that at finite temperature even after optimization the lowest free energy path is close to but does not coincide with the $z=0$ line. This can better seen if we assume that the tube width is small and therefore that terms higher than quadratic can be neglected in the z Taylor expansion of $F(s,z)$. Using this approximation we find that the tube width,

$$\langle z \rangle_s = \frac{\int e^{-\beta F(s,z)} z dz}{\int e^{-\beta F(s,z)} dz} \quad (6)$$

and the position of free energy minimum $z_{\min}(s)$ in z at fixed s coincide and are given by

$$\langle z \rangle_s \approx z_{\min}(s) = -\frac{\partial F(s,0)/\partial z}{\partial^2 F(s,0)/\partial z^2}, \quad (7)$$

thus confirming that out of necessity a finite tube width implies that $z_{\min}(s)$ is not zero. It is clear that this argument is fairly general and including terms higher than second order

one arrives at the conclusion that at finite temperature z_{\min} must be different from zero since the tube has finite width.

We can now return to the problem of exploring the paths whose existence is reflected in the appearance of the other valleys in the $F(s,z)$ surfaces far away from the $z=0$ line. First we choose the valley that we want to explore and then we connect a sequence of configurations lying at low free energy so as to form a new putative reaction coordinate. This will be used as an initial input for a new local optimization as described above. In such manner all possible relevant reaction coordinates can be sequentially explored.

The nature of the functions $s(\mathbf{R})$ and $z(\mathbf{R})$ is such that while for low values of z they provide a very fine topology capable of discriminating well among the different trajectories at large z they lead to a much coarser description. This consideration is unimportant for local optimizations where one deals only with the lower part of the (s,z) plane and the optimization procedure drives $\mathbf{R}(t)$ towards the horizontal axis thus improving the resolution but it might lead to an insufficient resolution of large z paths. However, our experience has so far shown this not to be the case and that the method proposed is an effective way of local and nonlocal explorations of low free energy paths.

III. DISCRETIZATION AND REPARAMETRIZATION

It has long been realized that in a path optimization procedure some form of reparametrization needs to be implemented.^{1,4} In order to make closer contact with applications we discuss the reparametrization procedure in the practical case in which the putative reaction coordinate $\mathbf{R}(t)$ is discretized. This implies that one writes Eqs. (1) and (2) as

$$s(\mathbf{R}) = \frac{1}{P-1} \frac{\sum_{i=1}^P (i-1) e^{-\lambda(\mathbf{R} - \mathbf{R}(i))^2}}{\sum_{i=1}^P e^{-\lambda(\mathbf{R} - \mathbf{R}(i))^2}} \quad (8)$$

and the corresponding z function as

$$z(\mathbf{R}) = -\frac{1}{\lambda} \ln \left(\sum_{i=1}^P e^{-\lambda(\mathbf{R} - \mathbf{R}(i))^2} \right), \quad (9)$$

where i is a discrete index ranging from 1 to P . In the present case $(\mathbf{R} - \mathbf{R}(i))^2$ is calculated as mean square displacement³⁹ but in other applications other types of metric might be considered. For the discrete representation to be meaningful it is necessary that the nodal points $\mathbf{R}(i)$ are as equidistant as possible and that λ is comparable to the inverse of mean square displacement between successive frames. In this way the function $s(\mathbf{R})$ increases smoothly from 0 to 1 along the path without discontinuities. With equidistant frames we can estimate \mathcal{T} using the trapezoidal rule,

$$\mathcal{T} = \frac{1}{P} \left[\frac{1}{2} (F(s(\mathbf{R}(1)), 0) + F(s(\mathbf{R}(P)), 0)) + \sum_{i=-2}^{P-1} F(s(\mathbf{R}(i)), 0) \right], \quad (10)$$

where the discretized definition of the variables $s(\mathbf{R})$ and $z(\mathbf{R})$ are used. Due to the need of maintaining the nodes

equidistant reparametrization needs extra care. Failing this the $s(\mathbf{R})$ function would present unphysical features when the nodes are further away than $1/\sqrt{\lambda}$ in root mean square displacement (RMSD) space. However, a saving grace when dealing with small P is that close to the nodes the coordinates s and z still work well especially in the direction perpendicular to the putative reaction coordinate and that this component of the force is what mostly drives the reaction coordinate towards the free energy minimum. This allows getting away with a small P with a fixed λ in the optimization process even when the mean internodal distance changes significantly. Different is the case of the evaluation of $F(s, z)$ which requires a smooth behavior of $s(\mathbf{R})$. For this part of the calculation either P or λ need to be changed to obtain correct results.

In order to keep the parameterization during the optimization we build on the NEB approach. There are several variants of NEB (Refs. 1–3) of progressive complexity and accuracy. The latest versions require explicit evaluation of PES for improving both saddle point estimates³ and tangent directions.² Since here we are working on the FES whose accurate values are difficult to calculate we are forced to the older variant¹ for which only the derivatives are needed. In NEB (Ref. 1) an artificial elastic energy term was introduced to help reparametrize the path,

$$E^{\text{NEB}} = \frac{1}{2} k \sum_{i=1}^{P-1} (\Delta \mathbf{R}_{i,i+1})^2, \quad (11)$$

where $\Delta \mathbf{R}_{i,i+1}$ is the root mean square displacement³⁹ between $\mathbf{R}(i)$ and $\mathbf{R}(i+1)$ and k is the elastic constant of the chain of springs. In our case E^{NEB} was not sufficient for our purposes and we found necessary to supplement the neighbor term in E^{NEB} with a non local term,

$$\begin{aligned} E^{\text{NET}} = & E^{\text{NEB}} + \frac{k}{4} \sum_{j=1}^{P-2} \sum_{k=j+2}^P (\Delta \mathbf{R}_{j,k} - \Delta \mathbf{R}_{j+1,k})^2 \\ & + \frac{k}{4} \sum_{j=1}^{P-2} \sum_{k=j+1}^{P-1} (\Delta \mathbf{R}_{j,k} - \Delta \mathbf{R}_{j,k+1})^2, \end{aligned} \quad (12)$$

which can be looked at as imposing a net of springs among all the nodes. The nonlocal terms have a more global effect on the final internodal distance and lead to a well behaved $s(\mathbf{R})$. We also note that a good measure of the ability of such reparametrization is the flatness of the surface spanned by the symmetric matrix $\Delta \mathbf{R}_{i,j}$ (Fig. 2). The flatter this surface, especially in the proximity of the diagonal elements, the better the parametrization. Using E^{NET} instead of E^{NEB} helps achieve this result. This is particularly relevant when P is a small number. When implemented on a test PES such as the modified London-Eyring-Polanyi-Sato potential in Ref. 1 the lowest energy path found was almost identical to the one obtained with the original NEB formulation.

As in NEB we need to identify the direction tangent to the curve. This is done via the following finite difference estimation of the tangent vector:¹

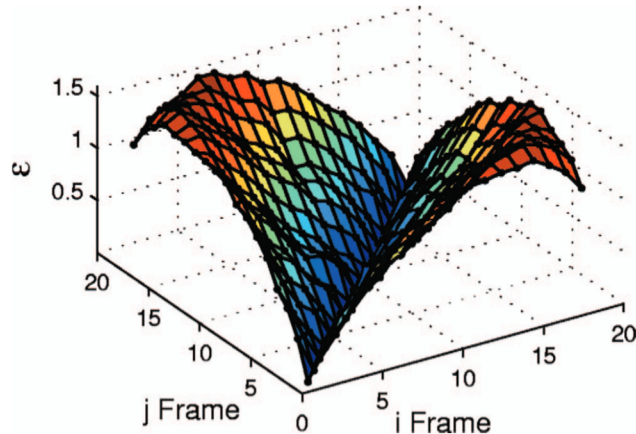


FIG. 2. (Color) Graphical representation of the root mean square matrix for the alanine dipeptide application.

$$\tau_i = \frac{1}{C} \left(\frac{\mathbf{R}(i+1) - \mathbf{R}(i)}{|\mathbf{R}(i+1) - \mathbf{R}(i)|} + \frac{\mathbf{R}(i) - \mathbf{R}(i-1)}{|\mathbf{R}(i) - \mathbf{R}(i-1)|} \right), \quad (13)$$

where C normalizes τ_i to 1. From now on the optimization procedure follows the NEB procedure and we update the position of the nodes using a steepest descent algorithm driven by the force

$$\begin{aligned} \mathcal{F}^{\text{tot}}[\mathbf{R}(i)] = & [\mathcal{F}^{\text{NET}}[\mathbf{R}(i)] \cdot \tau_i] \tau_i + [\mathcal{F}^{\text{str}}[\mathbf{R}(i)] \\ & - (\mathcal{F}^{\text{str}}[\mathbf{R}(i)] \cdot \tau_i) \tau_i], \end{aligned} \quad (14)$$

where $\mathcal{F}^{\text{NET}}[\mathbf{R}(i)]$ and $\mathcal{F}^{\text{str}}[\mathbf{R}(i)]$ are the spring and string tension derived forces, respectively. The difference from standard NEB lies not only in the different elastic energy but also in the object function which is not the energy but the string tension for which we do not have an explicit expression but which can only be estimated by statistical sampling. In practical applications we use the rule of thumb of choosing the spring constant k such that at the beginning of the calculation the elastic force approximately balances the thermodynamic one.

IV. AN EXAMPLE: DIALANINE IN VACUUM

As an example we show the application of the above described procedure to dialanine (ace-ala-nme) in vacuum, a typical system having multiple low free energy paths connecting different energy basins. For instance, it is known that the metastable conformers $C_{7\text{eq}}$ and C_{ax} (Refs. 34–36) can be connected by three different low free energy paths. Moreover this molecule has been extensively studied as test case for many computational techniques.^{25,31,40–42} Usually in this system the backbone dihedral angles Φ and Ψ are used as descriptors and the free energy is shown in the Ramachandran⁴³ plot (see Figs. 3 and 4, B panel).

The CHARMM27 (Ref. 44) force field has been used in version 4.0 of ORAC (Ref. 45) molecular dynamics code and velocity rescaling at 300 K as thermostat. In all simulations three atoms were constrained. In particular, we fixed the x component of the central nitrogen, the x and y components of hydrogen α , and the x , y , and z coordinates of the central C_α

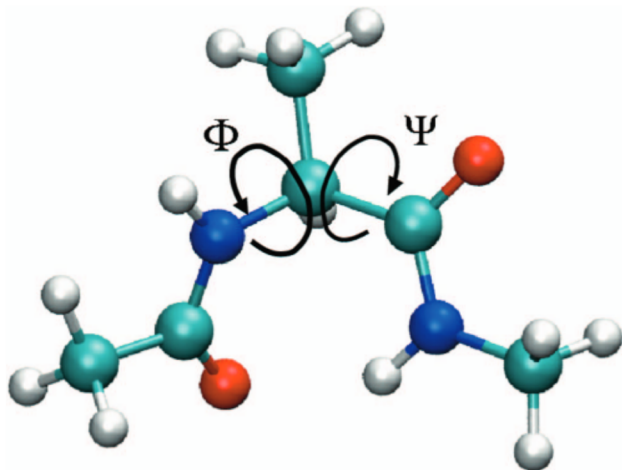


FIG. 3. (Color) Ball and stick representation of alanine dipeptide and definition of the Φ and Ψ dihedrals in the Ramachandran plot.

with a harmonic potential in order to hinder irrelevant rotations and translations.³²

In the s and z variables the evolution of the dialanine conformation is described by the Cartesian coordinate of the heavy atoms. The initial $\mathbf{R}(t)$ was obtained by linear interpolation between configurations $C_{7\text{eq}}$ and C_{ax} . We started with a low number of nodes $P=5$, and we later refined the calculation by increasing P , but good results were already obtained with such a low P . This rather unlikely path was chosen in order to prove the robustness of the method. In real applications a smarter choice would be more appropriate.⁴⁶ The value of λ was chosen to be 28.2 \AA^{-2} which ensured a good behavior of $s(\mathbf{R})$ and $z(\mathbf{R})$ and roughly corresponds to dividing the initial path length into P equal segments.

Metadynamics²² in its direct formulation³⁷ has been chosen to sample $F(s,z)$ surface. In this method one defines a fictitious dynamics in the space of the CV that is driven by the thermodynamic forces $dF(s,z)/ds$ and $dF(s,z)/dz$ (Ref. 47) and by a history dependent potential constructed by depositing repulsive Gaussians²¹ in the (s,z) points previously visited. It has been shown practically and theoretically that the sum of Gaussians provides an unbiased estimate of the underlying free energy.⁴⁸ The rate of Gaussian deposition can be very high ($1/60 \text{ fs}^{-1}$) given the fast equilibration of the degrees of freedom not included in $\mathbf{R}(t)$. The widths for Gaussians have been chosen to be 0.02 and 0.05 \AA^2 for z and s , respectively. The total simulation time for each metadynamics run was 3 ns .

Since the initial putative reaction coordinate is so unlikely, the low energy regions are to be found at high z and therefore these regions are the first to be filled by metadynamics. On $F(s,z)$ different valleys connecting $C_{7\text{eq}}$ with C_{ax} can be seen (see Fig. 4, A panel). Three low free energy paths can be identified: the yellow, the white, and the cyan. These are three well known pathways along which the conformational change from $C_{7\text{eq}}$ to C_{ax} can take place.^{35,40,49} For illustration purposes we have also calculated the free energy as a function of Φ and Ψ which is the conventional way of representing the free energy landscape of this system. On this two dimensional surface we mapped the $(3 \times 11 - 6)$ dimen-

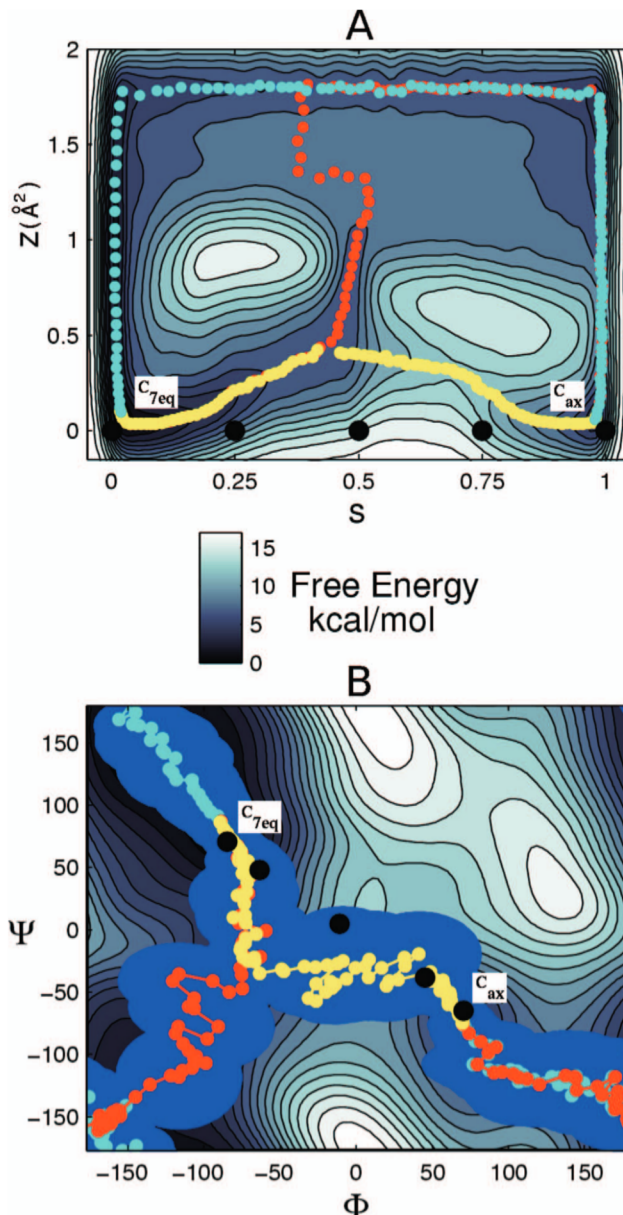


FIG. 4. (Color) Correspondence between minimum free energy paths between the s and z CVs (A panel) and Φ and Ψ dihedrals in Ramachandran plot representation (B panel). The isoline separation is 1.0 kcal/mol . Black dots represent points in the $\mathbf{R}(t)$ set on both (s,z) and Ramachandran plots. The minimum free energy paths found for the FES in (s,z) space (yellow, cyan, and red dots for different paths) have been plotted on the Ramachandran plot with relative uncertainty (blue cloud).

sional path (see Fig. 4, B panel). The mapping is obtained as follows. Every point within a window of 0.04 in s and 0.08 \AA^2 in z along the three paths represented in Fig. 4(a) results from an ensemble of microscopic configurations for which the average value of Φ and Ψ and the corresponding root mean square deviations are calculated. The set of these average values leads to paths on the Ramachandran plot shown in the B panel of Fig. 4, while the blue stripes surrounding the paths are graphical representations of uncertainties in Φ and Ψ . We stress once again that we use the Ramachandran plot as a way of representing in two dimensions what is really a multidimensional path.

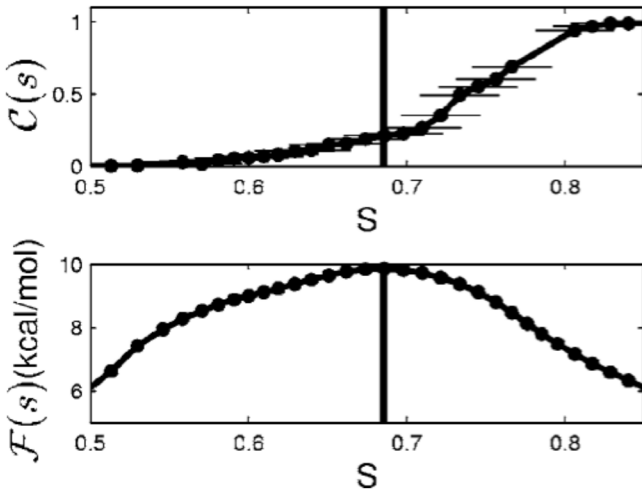


FIG. 5. Committor as a function of progress of the collective variable. Configurations within a z distance of 0.12 \AA^2 from the yellow path in Fig. 4(a) have been used. Committor values have been therefore calculated as a function of the progress along the path s . Limits for commitment in s and z space are $s < 0.1$ and $z < 0.2 \text{ \AA}^2$ for being committed to the $C_{7\text{eq}}$ basin; $s > 0.9$ and $z < 0.2 \text{ \AA}^2$ for being committed to the C_{ax} basin. An average of 2000 MD runs have been performed for each point. Horizontal lines on the curve in the upper panel indicate the width of sampling for each point.

The paths in Fig. 4(b) are very noisy but qualitatively similar to those previously reported.^{31,35,36,49} The position of the transition states in Fig. 4(a) as well as the corresponding barrier heights are also in agreement with previous estimates.^{31,49} However, this is rather fortuitous. In fact, as we shall show below, from the analysis of Ref. 31 we expect that, if the reaction coordinate is properly defined, one should find that at the transition state the committor function $C(s)$ has value $\frac{1}{2}$. In order to check this we calculated $C(s)$ by first selecting representative conformations along the low free energy path to which random velocities from the appropriate Maxwell distribution are assigned. From these initial conditions standard molecular dynamics (MD) trajectories are then run. The measured probability of ending up in, say, $C_{7\text{eq}}$ defines $C(s)$. The isocommittor point for which $C(s) = \frac{1}{2}$ is the natural definition of dynamical transition state.⁴⁰ It is seen that the apparent free energy saddle point does not coincide with the isocommittor as it should (see Fig. 5). This is also reflected in the projection of the putative transition state in the Ramachandran plot (see Fig. 6, A panel). Not only do most of the points lie to the left of the Φ and Ψ transition states but there is also a number of outliers. Thus the nodes \mathbf{R}_i need to be refined. In principle one could take a sequence of points from the yellow trajectory, use these as a new reference \mathbf{R}_i , and repeat the calculation. We prefer instead to use the string tension variational principle of Eq. (5).

V. A FIRST PATH OPTIMIZATION FOR ALANINE DIPEPTIDE

Starting from the linearly interpolated reaction coordinate with $P=5$ we evolved our string using a steepest-descent-like approach. At each evolution step a maximum of 0.05 \AA of root mean square displacement from previous frame is allowed for each $\mathbf{R}(i)$. The spring hardness was

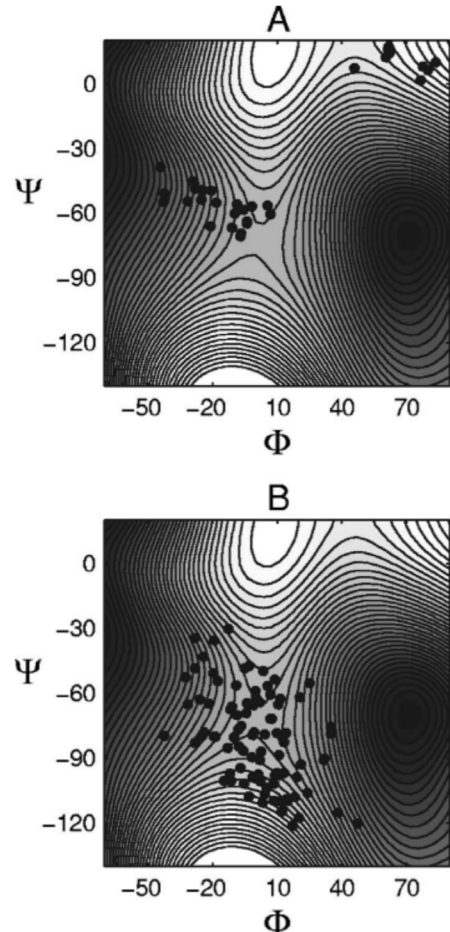


FIG. 6. Panel A: Ramachandran plot of the transition state zone including points before refinement in a slice from 0.6625 to 0.7125 along s in the minimum energy path and spanning 0.12 \AA^2 in z variable. When the putative reaction coordinate is the interpolation between $C_{7\text{eq}}$ and C_{ax} states, the saddle point is only approximately correct and is mixed with post-transition state configurations. Panel B: Ramachandran plot of points in transition state zone (in a slice from 0.7 to 0.75 along the s variable and spanning 0.12 \AA^2 in z variable) after refinement. The procedure corrects for the wrong transition state detected in panel A. Underlying free energy is represented with isolines separated by 0.25 kcal/mol.

tuned such that the net force was the same order of magnitude of the derivative of string tension. We checked convergence by monitoring the path length and the maximum value of the force. The path length was calculated by first aligning³⁹ all the frames to the initial one and integrating the spline⁵⁰ interpolated trajectory. After 60 iterations the string reached convergence within 1.6% of the path length. We believe that by using smarter optimization techniques this number could be substantially reduced. The effect of optimization is dramatic both in the (s, z) space and in the Ramachandran plot (see Fig. 7). There is now a free energy minimum much close to the $z=0$ axis, while in the (Φ, Ψ) plot the reaction coordinate is smoother.

Since the tube width is small we approximate the free energy profile with respect to s by its value at $z_{\min}(s)$ which is the closest minimum along z at fixed s ,

$$\mathcal{F}(s) \approx F(s, z_{\min}(s)). \quad (15)$$

It can be seen in Fig. 8 that contrary to the previous case (see Fig. 5) there is now a good correspondence between the

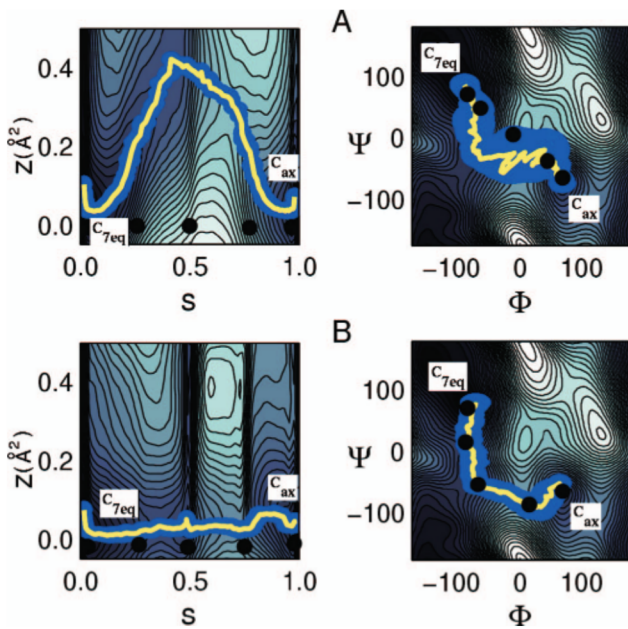


FIG. 7. (Color) A panels: Lowest free energy path (yellow line) for the interpolated path (represented as black dots) in both the (s, z) and its (Φ, Ψ) projection. B panels: The final minimum free energy path is almost overlapping with refined frames and uncertainty in Ramachandran plot (represented as blue stripe in the right panel) is much more reduced. Underlying free energy landscapes are represented with isolines separated by 0.5 kcal/mol and the color code is the same as Fig. 4.

saddle point in $\mathcal{F}(s)$ and the isocommittor point. Also a marked improvement is to be seen in the transition state ensemble. In the Ramachandran plot the transition state ensemble now straddles evenly the saddle point (see Fig. 6, B panel). The fact that the transition state ensemble is slanted relative to the watershed line reflects the fact noted by several authors^{25,32,40,42} that Φ and Ψ are only approximate reaction coordinates and need to be supplemented by other degrees of freedom for a correct description of the real reaction coordinate. In our case all these degrees of freedom are implicitly included.

VI. IMPROVING THE ACCURACY

In the previous section we have described a minimalistic implementation of our method. By this we mean that we

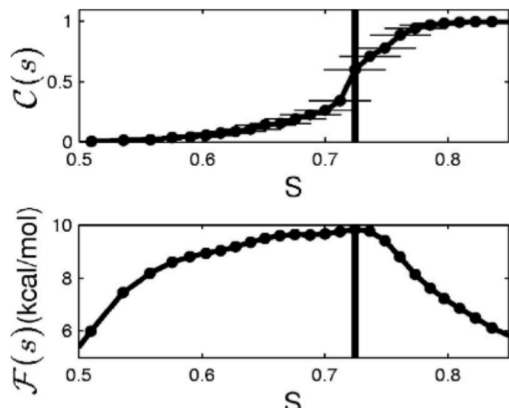


FIG. 8. Upper panel: Commitment probability as a function of progress of the s collective variable after refinement (see details in Fig. 5). At the end of refinement process the commitment probability for the saddle point in the FES (lower panel) is close to 0.5.

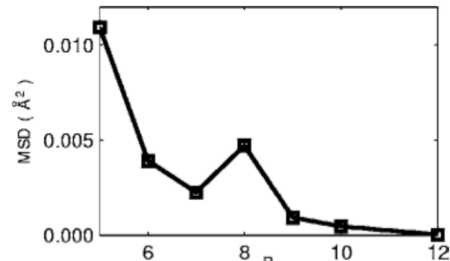


FIG. 9. Convergence is shown as function of mean deviation of each frame of the node set after alignment (Ref. 39) with respective points on the spline interpolated 12 node path.

have used a small P and evaluated the free energy along the putative reaction coordinate an approximate way from Eq. (15). Although the results are already satisfactory the accuracy of the calculation can be systematically improved. First we increase P from 5 to 12. Starting from the $P=5$ converged nodes we interpolate these points and extract 12 equidistant new nodes. As P increases for the same putative reaction coordinate the internodal distance shortens. Thus we use a bigger λ of 50.5 \AA^{-2} and repeat the calculation. Similar calculations have been performed with intermediate values of P . A fast convergence to a precision which is smaller than the tube width (about 0.02 \AA^2) is seen in Fig. 9. Although in the following sections we will present the results obtained with $P=12$ it is apparent that a smaller P would have been sufficient.

We now discuss the issue of how to calculate the free energy along the path in a more accurate way than the approximation of Eq. (15). In fact, one could use the standard definition,

$$\mathcal{F}(s) = -\frac{1}{\beta} \ln \int e^{-\beta V(\mathbf{R})} \delta(s(\mathbf{R}) - s) d\mathbf{R} \quad (16)$$

or

$$\mathcal{G}(s) = -\frac{1}{\beta} \ln \int |\nabla s(\mathbf{R})| e^{-\beta V(\mathbf{R})} \delta(s(\mathbf{R}) - s) d\mathbf{R}. \quad (17)$$

In the above two equations immaterial constants have been neglected and the integral is performed over all the degrees of freedom of the system \mathbf{R} . The second expression has been discussed in Ref. 51 and has two important properties. It remains invariant if instead of $s(\mathbf{R})$ one makes a change of variable to $f(s(\mathbf{R}))$ where f is a monotonic function as can be easily proved by direct substitution, and it is therefore gauge invariant.⁵¹ Furthermore one can rewrite Eq. (17) as

$$\mathcal{G}(s) = -\frac{1}{\beta} \ln \int e^{-\beta V(\mathbf{R})} d\sigma_s \quad (18)$$

where the integral is performed over the surface σ_s defined by $s(\mathbf{R}) = s$. In this equation the expression used in transition state theory to evaluate free energy barriers when s is the transition state coordinate can be easily recognized.

In the calculation of $\mathcal{F}(s)$ and $\mathcal{G}(s)$ limits have to be put on the range of integration in the direction perpendicular to the path. We therefore used

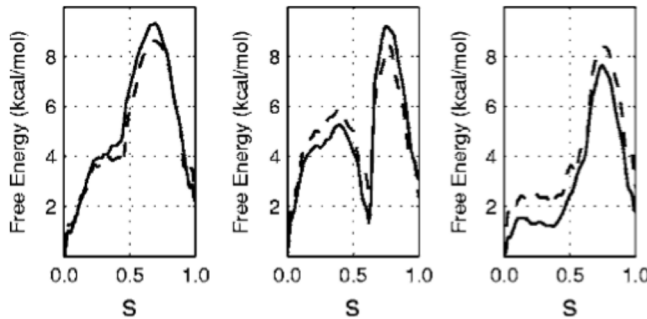


FIG. 10. Comparison with integrated FES up to $z=0.4$ for the gauge invariant (solid line) and traditional FES (dashed line) in all the three different paths. Shape of the curves, position of the minima, and transition states are the same.

$$\mathcal{F}(s) = -\frac{1}{\beta} \ln \frac{\int_0^{z_{\max}} e^{-\beta F(s,z)} dz}{Z}, \quad (19)$$

where $z_{\max} \approx 0.4 \text{ \AA}^2$ which is larger than the tube size and still small enough not to include contributions from other low energy paths. We also calculated $\mathcal{G}(s)$ by noting that it can be written as

$$\mathcal{G}(s) = -\frac{1}{\beta} \ln \int e^{-\beta(V(\mathbf{R}) - \ln|\nabla s(\mathbf{R})|/\beta)} \delta(s(\mathbf{R}) - s) d\mathbf{R}, \quad (20)$$

that is to say, one can calculate $\mathcal{G}(s)$ as one does $\mathcal{F}(s)$ but using the modified potential

$$V(\mathbf{R}) - \frac{\ln|\nabla s(\mathbf{R})|}{\beta} \quad (21)$$

rather than the original $V(\mathbf{R})$.

In Fig. 10 we compare these ways of calculating the free energy. They are all reassuringly similar with most of the change coming from regions close to the initial and final points of $\mathbf{R}(t)$. Of particular value is the observation that $\mathcal{F}(s)$ and $\mathcal{G}(s)$ are numerically close. In fact the modified potential in Eq. (21) would substantially differ from the original $V(x)$ if the radius of curvature of the path were small. Since the variables $s(\mathbf{R})$ and $z(\mathbf{R})$ are based on the assumption of large curvature radii this gives additional confidence in our results. Furthermore, given the fact that the putative reaction coordinate evolution can be viewed in some sense as a particular kind of gauge transformation, the similarity of the two curves ensures that our reparametrization procedure preserves the physical meaning of our variables without introducing distortions.

In other words this implies that our original parametrization is still reasonable even after $\mathbf{R}(t)$ evolution and that the radius of curvature of the putative reaction coordinate remains large such that the assumption that $s(\mathbf{R})$ and $z(\mathbf{R})$ isosurfaces are planes and tubes, respectively, still holds in a large enough region around the path.

VII. THE FULL PICTURE

We can now finally put together the results for all the three paths: the yellow, the red, and the cyan. We present only results with $P=12$. The initial $\mathbf{R}(t)$ for the cyan and red paths were obtained by selecting approximately equidistant

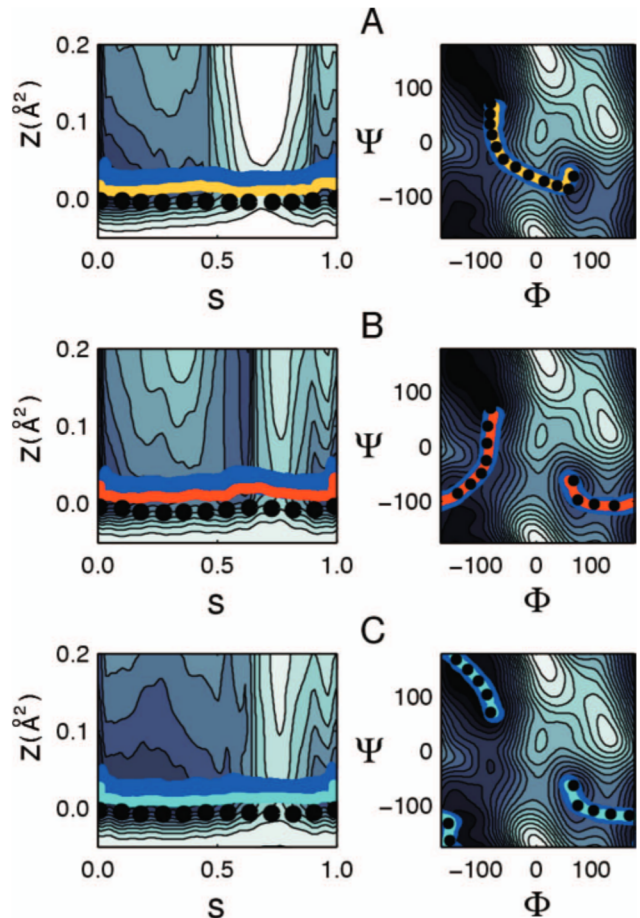


FIG. 11. (Color) Three different paths calculated by optimizing the string tension with $P=12$. Left panels: Black dots represent the optimized reference frames. Color lines are the computed minimum free energy paths calculated in both (s,z) and projected on the (Φ,Ψ) space (right panels). Their standard deviations within a stripe along minimum free energy paths in (s,z) are projected on (Φ,Ψ) space and reported as blue stripes surrounding the paths. In all the panels the underlying free energy surfaces are represented with isolines each 1 kcal/mol and the color code is the same as in Fig. 4.

frames from the low free energy paths obtained in our first simulation shown in Fig. 4. The λ values used during the optimization were calculated by dividing the length of the path by P and were $\lambda=39.8 \text{ \AA}^{-2}$ and $\lambda=24.8 \text{ \AA}^{-2}$ for the red and the cyan paths, respectively. At the end of this procedure, internodal distances changed. Thus in the $F(s,z)$ calculations we chose $\lambda=64.0 \text{ \AA}^{-2}$, $\lambda=24.8 \text{ \AA}^{-2}$, and $\lambda=27.0 \text{ \AA}^{-2}$ for the yellow, the red, and the cyan, respectively. The results are collected in Fig. 11 and show that the method converges well in all three cases and gives a global view of the three dominant low free energy paths. The left panels cannot be directly compared since they are calculated relative to different reference $\mathbf{R}(t)$'s. They, however, show good convergence in all cases, and the curve $z_m(s)$ is very close to the $z=0$ line which implies that the tube diameter is small. In Fig. 12 we plot the free energy profile and the committor. We clearly find that within the accuracy of the calculation in all three paths the transition state has a dynamical meaning since it is located very closely to the isocommittor point. The transition state ensemble for our most accurate calculations are finally shown in Fig. 13 and are in good agreement with previous studies.

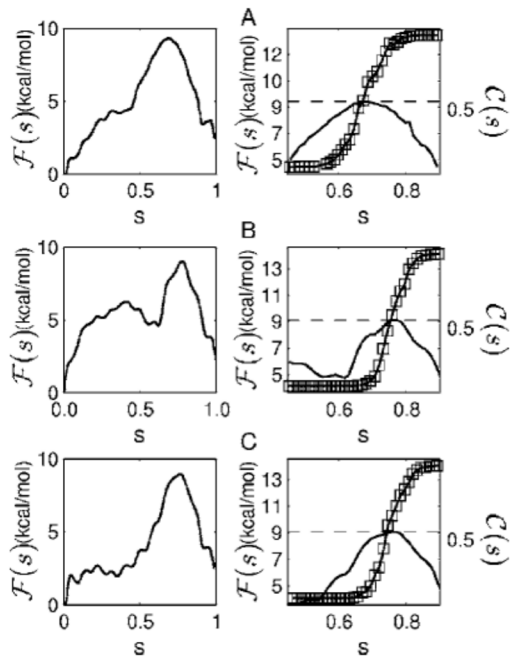


FIG. 12. On the left the free energy profiles after optimization for the paths projected over s and integrated up to $z(s)=2 \times z_{\min}(s)$. Commitment analysis after optimization for all the three low energy paths. On the right: Top of free energy profiles are shown in such a way that the dashed lines representing the isocommittor are aligned with putative transition states. In all three cases the isocommittor values coincide with the supposed transition states. On the right side of each plot the committor $C(s)$ scale is represented, while on the left side the free energy scale for the overlapping FESs is provided. The width of sampling in s for each point of committor is equal to the square marker width while in z is $2 \times z_{\min}(s)$.

VIII. CONCLUSION

In this paper we have presented a novel method for studying low energy paths at finite temperature. The method combines features of path finding and collective variable approaches. A method for the local optimization of low free energy paths is highly competitive. However, its most appealing and potentially revolutionary feature is that it is capable of nonlocal exploration and is able to find transition low free energy paths unrelated to the initial guess. In fact, not even the final state needs to be known precisely for the method to work. The method has relative simplicity of implementation and has a flexibility which will be explored in the future. For instance, it will be easy to introduce a description of the path in terms of collective variables rather than Cartesian coordinates or else to consider more sophisticated metrics. The ability to find very reasonable results with a scaled down version of the theory, that is, with low P and approximate estimate of the free energy might prove a strong asset when dealing with very large and computationally demanding systems.

ACKNOWLEDGMENTS

The authors thank Alessandro Laio for providing us with the RMSD routine and helpful discussions at the early stages of this project. They also thank Giovanni Bussi for useful discussions.

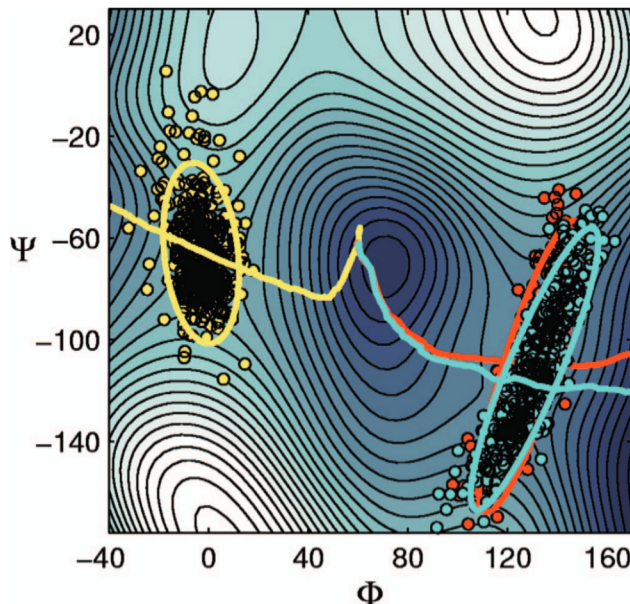


FIG. 13. (Color) Representation of the saddle points along s within 0.4 \AA^2 in z for each path in the Ramachandran plot. Ellipsoids indicate the direction of dispersion on the values and minimum free energy paths are represented as solid lines. The major axis of yellow ellipsoid is not orthogonal to the relative minimum free energy path and must be supplemented by other variables involved in the transition (Ref. 32 and 40) (isoline separation: 0.5 kcal/mol, color code as in Fig. 4).

- ¹H. Jonsson, G. Mills, and K. W. Jacobsen, *Classical Dynamics in Condensed Phase Simulations*, edited by B. J. Berne, G. Ciccotti, and D. F. Coker (World Scientific, Singapore, 1998), p. 385.
- ²G. Henkeman and H. Jonsson, *J. Chem. Phys.* **113**, 9978 (2000).
- ³G. Henkeman, B. P. Uberuaga, and H. Jonsson, *J. Chem. Phys.* **113**, 9901 (2000).
- ⁴W. E. W. Ren, and E. Vanden-Eijnden, *Phys. Rev. B* **66**, 52301 (2002).
- ⁵P. G. Bolhuis, C. Dellago, and D. Chandler, *Faraday Discuss.* **110**, 421 (1998).
- ⁶P. G. Bolhuis, D. Chandler, C. Dellago, and P. L. Geissler, *Annu. Rev. Phys. Chem.* **53**, 291 (2002).
- ⁷D. Passerone and M. Parrinello, *Phys. Rev. Lett.* **87**, 108302 (2001).
- ⁸D. Passerone, M. Ceccarelli, and M. Parrinello, *J. Chem. Phys.* **118**, 2025 (2003).
- ⁹A. K. Faradjian and R. Elber, *J. Chem. Phys.* **120**, 10880 (2004).
- ¹⁰E. A. Carter, G. Ciccotti, J. T. Hynes, and R. Kapral, *Chem. Phys. Lett.* **156**, 472 (1989).
- ¹¹M. Sprak and G. Ciccotti, *J. Chem. Phys.* **109**, 7737 (1998).
- ¹²G. N. Patey and J. P. Valleau, *J. Chem. Phys.* **63**, 2334 (1975).
- ¹³A. M. Ferrenberg and R. H. Swendsen, *Phys. Rev. Lett.* **61**, 2635 (1988).
- ¹⁴S. Kumar, J. M. Rosenberg, D. Bouzida, R. H. Swendsen, and P. A. Kollman, *J. Comput. Chem.* **16**, 1339 (1995).
- ¹⁵B. Roux, *Comput. Phys. Commun.* **91**, 275 (1995).
- ¹⁶C. Jarzynski, *Phys. Rev. Lett.* **78**, 2690 (1997).
- ¹⁷E. Darve and A. Pohorille, *J. Chem. Phys.* **115**, 9169 (2001).
- ¹⁸H. Grubmüller, *Phys. Rev. E* **52**, 2893 (1995).
- ¹⁹F. A. Voter, *Phys. Rev. Lett.* **78**, 3908 (1997).
- ²⁰D. Cvijovic and J. Klinowski, *Science* **267**, 664 (1995).
- ²¹T. Huber, A. E. Torda, and W. F. van Gunsteren, *J. Comput.-Aided Mol. Des.* **8**, 695 (1994).
- ²²A. Laio and M. Parrinello, *Proc. Natl. Acad. Sci. U.S.A.* **20**, 12562 (2002).
- ²³B. Ensing, A. Laio, M. Parrinello, and M. L. Klein, *J. Phys. Chem. B* **109**, 6676 (2005).
- ²⁴B. Ensing and M. L. Klein, *Proc. Natl. Acad. Sci. U.S.A.* **102**, 6755 (2005).
- ²⁵L. Maragliano, A. Fischer, and E. Vanden-Eijnden, *J. Chem. Phys.* **125**, 024106 (2006).
- ²⁶P. J. Steinhardt, D. R. Nelson, and M. Ronchetti, *Phys. Rev. Lett.* **47**, 1297 (1981).

- ²⁷M. Iannuzzi, A. Laio, and M. Parrinello, *Phys. Rev. Lett.* **90**, 238302 (2003).
- ²⁸W. E, W. Ren, and E. Vanden-Eijnden, *J. Appl. Phys.* **93**, 2275 (2003).
- ²⁹D. H. Mathews and D. A. Case, *J. Mol. Biol.* **357**, 1683 (2006).
- ³⁰M. R. Sorensen, M. Brandbyge, and K. Jacobsen, *Phys. Rev. B* **57**, 3283 (1998).
- ³¹W. E, W. Ren, and E. Vanden-Eijnden, *J. Phys. Chem. B* **109**, 6688 (2005).
- ³²W. Ren, E. Vanden-Eijnden, P. Maragakis, and W. E, *J. Chem. Phys.* **123**, 134109 (2005).
- ³³D. Moroni, P. G. Bolhuis, and T. S. van Erp, *J. Chem. Phys.* **120**, 4055 (2004).
- ³⁴C. Bartels and M. Karplus, *J. Comput. Chem.* **18**, 1450 (1997).
- ³⁵J. Apostolakis, P. Ferrara, and A. Caflisch, *J. Chem. Phys.* **110**, 2099 (1999).
- ³⁶T. Lazaridis, D. J. Tobias, C. L. Brooks, and M. E. Paulaitis, *J. Chem. Phys.* **95**, 7612 (1991).
- ³⁷A. Laio, A. Fortea-Rodriguez, F. L. Gervasio, M. Ceccarelli, and M. Parrinello, *J. Phys. Chem. B* **109**, 6714 (2005).
- ³⁸P. Raiteri, A. Laio, F. L. Gervasio, C. Micheletti, and M. Parrinello, *J. Phys. Chem. B* **110**, 3533 (2006).
- ³⁹S. K. Kearsley, *Acta Crystallogr., Sect. A: Found. Crystallogr.* **45**, 208 (1989).
- ⁴⁰P. G. Bolhuis, C. Dellago, and D. Chandler, *Proc. Natl. Acad. Sci. U.S.A.* **97**, 5877 (2000).
- ⁴¹R. Crehuet and M. J. Field, *J. Chem. Phys.* **118**, 9563 (2003).
- ⁴²A. Ma and A. R. Dinner, *J. Phys. Chem. B* **109**, 6769 (2005).
- ⁴³G. N. Ramachandran, C. Ramakrishnan, and V. Sasisekharan, *J. Mol. Biol.* **7**, 95 (1963).
- ⁴⁴A. D. MacKerell, Jr., D. Bashford, M. Bellott *et al.*, *J. Phys. Chem. B* **102**, 3586 (1998).
- ⁴⁵P. Procacci, T. A. Darden, E. Paci, and M. Marchi, *J. Comput. Chem.* **18**, 1848 (1997).
- ⁴⁶M. Gerstein and W. Krebs, *Nucleic Acids Res.* **26**, 4280 (1998).
- ⁴⁷C. W. Gear, I. G. Kevrekidis, and C. Theodoropoulos, *Comput. Chem. Eng.* **26**, 941 (2002).
- ⁴⁸G. Bussi, A. Laio, and M. Parrinello, *Phys. Rev. Lett.* **96**, 090601 (2006).
- ⁴⁹P. E. Smith, *J. Chem. Phys.* **111**, 5568 (1999).
- ⁵⁰E. Catmull and R. Rom, *Computer Aided Geometric Design* (Academic, New York, 1974).
- ⁵¹W. E and E. Vanden-Eijnden, *Multiscale Modelling and Simulation*, edited by S. Attinger and P. Komoutsakos (Springer, New York, 2004).